Structural constraints on the spatial distribution of aftershocks

John McCloskey, Süleyman S. Nalbant, and Sandy Steacy
Geophysics Research Group, University of Ulster, Coleraine, Ireland

Concetta Nostro
Istituo Nazionale di Geofisica et Volcanologia, Roma, Italy

Oona Scotti and David Baumont
IRSN, Fontenya-Aux-Roses, France

[1] Calculations of static stress changes due to large earthquakes have shown that the spatial distribution of aftershocks is predictable to first order, with aftershocks primarily occurring in areas experiencing positive stress changes. Delineation of these areas relies on resolving the stress perturbation onto planes with known orientations; common practice is to use poorly constrained regional stress information to compute optimally oriented failure planes, assuming that they exist everywhere. Here we show that this assumption is not supported by observation but rather that aftershock failure planes are controlled by geological structure. We argue that useful aftershock hazard estimates are better made by replacing information on regional stress with statistical measures of structural orientations.   INDEX TERMS: 7209 Seismology: Earthquake dynamics and mechanics; 7223 Seismology: Seismic hazard assessment and prediction; 7230 Seismology: Seismicity and seismotectonics. **Citation:** McCloskey, J., S. S. Nalbant, S. Steacy, C. Nostro, O. Scotti, and D. Baumont, Structural constraints on the spatial distribution of aftershocks, *Geophys. Res. Lett.*, *30*(12), 1610, doi:10.1029/2003GL017225, 2003.

1. Introduction

[2] It is now widely acknowledged that the deterministic prediction of the time, location and magnitude of a future damaging earthquake is unlikely to be achieved in the short term [*Main*, 1997]. More frequently, now, earthquake scientists attempt to measure temporal and spatial variations in underlying hazard distributions and thereby assess the seismic outlook in a study area [*Stein et al.*, 1997; *Toda et al.*, 1998; *Nalbant et al.*, 1998; *Hubert-Ferrari et al.*, 2000; *Nalbant et al.*, 2002]. Of particular promise in this respect is the so-called Coulomb Stress Technique (CST) in which changes of the state of stress on a fault due to interaction with activity on neighbouring faults are calculated and resulting changes in failure probability are estimated [*Stein et al.*, 1997; *Toda et al.*, 1998; *Toda and Stein*, 2002].

[3] The CST was initially developed to explain aftershock distributions, notably following the Landers (M = 7.3) earthquake [*Stein et al.*, 1992; *King et al.*, 1994]. Indeed many aspects of the hazard problem are greatly simplified immediately following a large earthquake when the occurrence of aftershocks in time and space is causally related to that earthquake and is closely controlled by it. Aftershocks are also of significant social interest since they occur in a space-time window in which building stock is already weakened and they can, therefore, cause damage which is disproportionate to their size. The assessment of the likely spatial distribution of aftershocks in real time following a large earthquake could be of significant social benefit and might fall within the scientific scope of the CST.

[4] The stress state of an active fault can be described by its Coulomb stress, CS, given by $CS = \tau - \mu'\sigma_n$ where τ is the shear stress on the fault, σ_n is the normal stress and μ' is the coefficient of effective friction which includes the influences of both mechanical friction and pore fluid pressure. While it is not possible to measure CS directly, changes in CS due to neighbouring earthquakes (ΔCS) may be calculated by summing the stress changes due to all slipping fault patches and resolving the resulting stress perturbation tensor (SPT) onto the plane(s) of interest. In this way it was possible, for example, to identify the epicentral region of the M = 7.4 Izmit earthquake which caused extensive devastation and loss of life in Turkey in 1999 more than a year in advance of the event [*Stein et al.*, 1997; *Nalbant et al.*, 1998]. The assumptions that govern the selection of these planes is made have significant effects on the planes' orientations and, therefore, on the estimated hazard distribution. Here we address the nature of these fundamental assumptions.
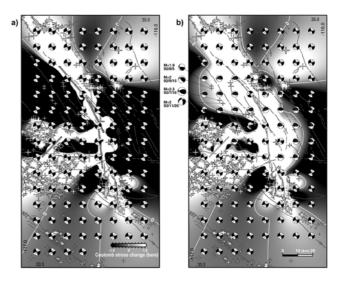
[5] If this technique is to be used as a practical tool for real time hazard estimation following a damaging earthquake a sequence of measurements, calculations and judgements must be made immediately after the event and continuously updated as time progresses. Estimates of the slip distribution of an earthquake might be made within a few hours of a large earthquake and used quickly to calculate the SPT in the region. This SPT might then be updated over the days or weeks as better quality data became available following the mainshock, giving a constantly evolving picture of the aftershock hazard. In the most common version of the CST, the SPT is combined with the regional stress tensor and the total stress is used to calculate planes optimally oriented for failure (OOPs) at every point of interest [*King et al.*, 1994; *Nalbant et al.*, 1998; *Hubert-Ferrari et al.*, 2000]. The orientations of the OOPs are strongly dependent on the orientation of the

regional stress field, which can vary widely even in reasonably simple, and intensively studied geologic systems such as Southern California [*Jennings*, 1994]. The advantage of the method is that it makes it possible to create hazard maps for the region surrounding a large earthquake in the absence of any knowledge of the local structural geology. The structure is in fact inferred from the regional stress field.

2. Coulomb Stress, Fault Structure, and Earthquakes

[6] Figure 1a shows the, now familiar, results of this procedure for the Landers earthquake. To produce this diagram, we begin by computing SPTs using the finite-fault source model of *Wald and Heaton* [1994], embedded in an elastic half-space with Poisson's ration 0.25 and Young's modulus 75 GPa. We then combine these SPTs with the regional stress field $\sigma_1 = 100$ bars, oriented N7°E, and $\sigma_2 = 5$ bars, oriented vertically [*King et al.*, 1994; *Hardebeck and Hauksson*, 2001], to estimate the orientations of the OOPs. We compute the OOPs in a 3D stress field, but constrain the solutions to occur on vertical structures (referred to here as a 2.5D solution); beach-balls represent the vertical strike-slip mechanisms which we use to calculate the colours on the map [*Stein et al.*, 1992; *King et al.*, 1994]. We then resolve the SPTs on the OOPs at an intermediate depth of 6.5 km using the high value of $\mu' = 0.8$ favoured by *Parsons and Dreger* [2000]. We note that our main conclusions do not change appreciably when σ_2 is doubled or μ' is reduced to 0.4. The grey crosses, which indicate the locations of observed aftershocks, show that the technique results in an accurate prediction of their spatial distribution.

[7] Figure 1b shows the same picture when we remove the vertical structural constraint and allow 3D optimally oriented planes with any focal mechanism. It is clear that this figure contains additional areas in which aftershocks are encouraged in addition to those encouraged in the restricted mechanism case (Figure 1a). These regions exist because, although vertical strike-slip mechanisms are discouraged by the 3-D stress perturbation, other mechanisms, notably, in this case, thrust mechanisms to the north-west and to the east of the epicenter, are encouraged. Inspection of the fault plane solutions of the few events occurring in these regions (beach-balls in the margins of Figure 1b) shows that these thrust mechanisms are actually observed, although in these regions aftershocks are in general very uncommon and quite small (M ≤ 2.5). Paradoxically, since the aftershock locations now cover a smaller percentage of the encouraged regions, this more rigorous calculation, which successfully predicts the observed non-strike-slip mechanisms, has actually decreased the effectiveness of the CST in estimating the seismic hazard.

[8] This paradox is explained by examining the relationship between predicted seismicity, observed seismicity and geological structure in the region before and after the Landers earthquake. Using the digital fault map of the area [*California Department of Conservation*, 2000] the faults in the region depicted in Figure 1, which exhibit Quaternary, Holocene or historical activity, are discretized at a resolution of 1 km. The distribution of the orientations of these fault increments is shown as a rose diagram in the upper semicircle of Figure 2. Generally, the faults have NW−SE orientations although a

Figure 1. Maps of ΔCS surrounding the Landers earthquake. Background colors represent values of ΔCS on optimally oriented planes. Fine lines on diagrams represent mapped structure. White crosses indicate location of all aftershocks with M > 2.0 occurring more than 5 km from the main rupture within 1.0 year following the mainshock. (a) 2.5D solution allowing only vertical strike-slip mechanisms. (b) 3D solutions in which permitted mechanisms are unconstrained. Note additional regions of failure enhancement in b due to possibility of thrust events to the NW and SE of the epicenter. Mechanisms of aftershocks in these additional regions are shown in the margins. L, Landers rupture plane(s); BB, Big Bear rupture plane and JT, Joshua Tree rupture plane.

small number of approximately east west structures are present. Examination of the structural map of the area [*Jennings*, 1994] shows that the dominant NW−SE structures are almost entirely vertical strike-slip faults which have a mean orientation of 329°N (the black arrow in Figure 2) and a 1σ range of ±22°. This area has a strong structural fabric dominated by NW−SE, vertical, strike-slip faults. The E−W structures, which represent an outlier to this fabric, are more variable and include a number of thrust faults. The observed seismicity in the 21 years prior to the Landers earthquake is shown in the lower semicircle of the same figure. We choose the nodal plane from the focal mechanism which is closest to the main structural trend; the vector mean of these orientations (the gray arrow in Figure 2) lies within 6 degrees of the structural mean, and therefore the seismicity prior to the Landers event is completely explained by the local structure. The mechanisms [*Hauksson*, 2000] are predominantly vertical strike-slip with strikes in almost the same range as the main structural set. There are also a few small thrust events with strikes generally in the E−W range, again entirely consistent with the mapped structure.

[9] Figure 3 shows the situation for the aftershocks in the year following Landers. The rose diagram in the upper semicircle is identical to that in Figure 2. Encouraged focal mechanisms fall into two broad categories, which are numerically equal within a factor of about two; vertical, strike-slip mechanisms which cluster around the circumference at strikes of about 340°N, and two groups of thrust
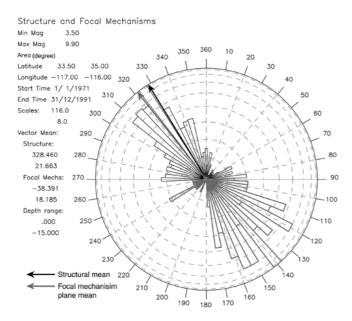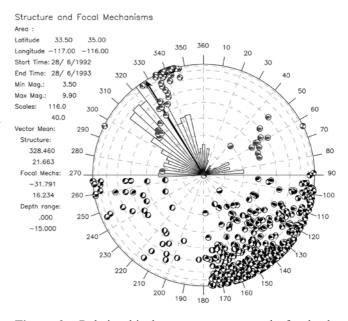
Figure 2. Relationships between predicted seismicity, observed seismicity and mapped structure in study area. Rose diagrams in the upper semicircle represent the distribution of orientations of structure which has experienced recent (Quaternary, Holocene or historical) seismicity. (Note that 180° is added to fault strike, if necessary, to ensure that all orientations plot in upper semicircle). Radial length of the bars is proportional to the number of 1 km structural elements in each particular orientation, the maximum value is 116. Black arrow indicates the mean structural orientation. Rose diagram in lower semicircle represents distribution of earthquake orientations in the 21 years preceding Landers event where the nodal plane most closely aligned with the structure is chosen (Note that here 180° is subtracted from event strike if necessary). Here the radial length of the bars is proportional to the number of events in each orientation, the maximum is 8. Vector mean is plotted in gray in upper semicircle, note that it is within 7° of the mean structural trend.

events which dip about 40–50 degrees. The observed seismicity is plotted in the lower semicircle and has changed very little from the pre-Landers data, again falling predictably around the dominant structural orientations with the great majority of mechanisms being vertical, strike-slip striking between 110° and 180°N and with a vector mean, as calculated for the preshocks of 328 degrees. The correspondence between these events and the mapped structure is impressive and the data are not consistent with a significant regional stress rotation due to the mainshock. We also note the expected order of magnitude increase in rate for these events. In contrast to the situation for the strike-slip events, however, we see only a small number of thrust events which are largely responsible for the increased size of the enhanced areas in Figure 1b as compared to Figure 1a. It is clear that while the OOPs in the these regions of Figure 1b are E–W striking thrust faults which dip at about 45 degrees, only a very few of these structures exist and, in general, aftershocks with these mechanisms are not observed. These results demonstrate that planes of weakness, optimally oriented for failure in this stress field, do not exist

everywhere and that the aftershock population is controlled by structure and not by stress. The pre-existing fabric in the area appears to act as a structural keel anchoring the aftershock orientations against the variations in the stress.

3. Discussion

[10] Can we use this result to improve hazard estimation, employing fault information to constrain the planes onto which ΔCS is computed? Since the correspondence between observed seismicity and mapped structure is so good, we expect that a Coulomb stress map based on observed structure would successfully predict the areas of aftershock activity. We test this idea by identifying the optimally oriented structures (OOSs) within the restricted range as defined by the structural data; at each point in the region we assume that all structure on which aftershocks will occur is consistent with the regional fabric exposed in Figure 2 and hence we compute ΔCS on a suite of right-lateral strike-slip fault planes with orientations ranging from 323–335° and choose the plane with the highest value. Note that while an OOP is a mathematical construction which does not exist in reality, an OOS is a statistical estimate of the real structure which will experience the greatest stress increase due to a given stress perturbation. Figure 4 shows the result of this calculation where 88.6% of aftershocks occur in regions of positive Coulomb stress change as compared to the 79.1% that did so using the OOP method illustrated in

Figure 3. Relationship between structure and aftershock mechanism. Rose diagram in the upper semicircle illustrates the same distribution of strike-slip faults observed in region shown in Figure 2. Gray beach-balls in the upper semicircle represent focal mechanisms on OOP's as predicted by CST and shown in Figure 1b. Beach balls are plotted on the diagram based on the orientation of the nodal plane which has experienced the greatest stress increase, the azimuth gives the strike and the distance from the center the dip, vertical planes plot on the outer rim of the diagram. Black beach-balls in the lower semicircles represent focal mechanisms of observed earthquakes occurring after the Landers event.
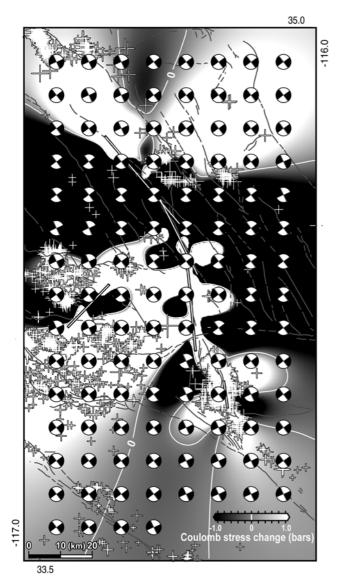
Figure 4. Map of ΔCS calculated on failure planes constrained by the regional structural trend illustrated in Figure 2b. Coulomb stress is calculated on a regular grid for a suite of right-lateral strike-slip planes dipping 90° and ranging in orientation between 323° and 335°; the maximum value is plotted at each point. In comparison to Figure 1a, note that a greater percentage of aftershocks occur in regions of positive Coulomb stress change yet the technique is independent of knowledge of a poorly constrained regional stress field.

Figure 1a. The greatest change is in the SW of the region. This is crucially important as this new method is based solely on fault geometry, and hence does not require knowledge of a poorly constrained regional stress field.

[11] There are important consequences here for the use of the CST in the forward modeling of aftershock populations. It would appear that the apparently remarkable success of the OOP idea in predicting the spatial distribution of the aftershocks to the Landers event resulted from the inclusion of a vital piece of geological insight. In constraining the focal mechanisms to be vertical strike-slip the dominance of vertical strike-slip faulting in the region was implicitly included and all other mechanisms, which could not in fact have been supported by the available structure, were suppressed in the calculations. The spatial distribution of the events fitted the prediction accurately. In general, and in regions of more complex tectonics in particular, this implicit constraint is unlikely to be employed and a more systematic inclusion of structural information would appear to be required. We propose that statistical measures of existing geological structure should be combined with the OOP idea so that the optimal is constrained by the possible, in other words that the most likely failure plane is chosen within the range of observed possible failure planes.

References

California Department of Conservation, Digital database of faults from the fault activity map of California and adjacent areas, Div. of Mines and Geol. publication CD 2000-006, Sacramento, 2000.

Hardebeck, J. L., and E. Hauksson, Crustal stress field in southern California and its implications for fault mechanics, *J. Geophys. Res.*, *106*, 21,859–21,882, 2001.

Hauksson, E., Crustal structure and seismicity distribution adjacent to the Pacific and North America plate boundary in southern California, *Journal Geophys. Res.*, *105*, 13,875–13,903, 2000.

Hubert-Ferrari, A., A. Barka, E. Jacques, S. S. Nalbant, B. Meyer, R. Armijo, P. Tapponnier, and G. C. P. King, Seismic hazard in the Marmara Sea region following the 17 August 1999 Izmit earthquake, *Nature*, *404*, 269–273, 2000.

Jennings, C. W., Fault activity map of California and adjacent areas, 1:750,000 scale, Calif. Div. of Mines and Geol., Geologic Data Map No. 6, Sacramento, 1994.

King, G. C. P., R. S. Stein, and J. Lin, Static stress changes and the triggering of earthquakes, *Bull. Seismol. Soc. Amer.*, *84*, 935–953, 1994.

Main, I., Long odds on prediction, *Nature*, *385*, 19–20, 1997.

Nalbant, S. S., A. Hubert, and G. C. P. King, Stress coupling between earthquakes in northwest Turkey and the north Aegean Sea, *Journal Geophys. Res.*, *103*, 24,469–24,486, 1998.

Nalbant, S. S., J. McCloskey, S. Steacy, and A. Barka, Stress accumulation and increased seismic risk in Eastern Turkey, *Earth Planet. Sci. Lett.*, *195*, 291–298, 2002.

Parsons, T., and D. S. Dreger, Static-stress impact of the 1992 Landers earthquake sequence on nucleation and slip at the site of the 1999 M = 7.1 Hector Mine earthquake, southern California, *Geophys. Res. Lett.*, *27*, 1949–1952, 2000.

Stein, R. S., G. C. P. King, and J. Lin, Change in failure stress on the southern San Andreas fault system caused by the 1992 Magnitude = 7.4 Landers earthquake, *Science*, *258*, 1328–1332, 1992.

Stein, R. S., A. A. Barka, and J. H. Dieterich, Progressive failure on the North Anatolian fault since 1939 by earthquake stress triggering, *Geophys. J. Int.*, *128*, 594–604, 1997.

Toda, S., and R. S. Stein, Response of the San Andreas Fault to the 1983 Coalinga-Nuñez Earthquakes: An Application of Interaction-based Probabilities for Parkfield, *J. Geophys. Res.*, *107*, 10.1029/2001JB000172, 2002.

Toda, S., R. S. Stein, P. A. Reasenberg, and J. H. Dieterich, Stress transferred by the Mw = 6.9 Kobe, Japan, shock: Effect on aftershocks and future earthquake probabilities, *J. Geophys. Res.*, *103*, 24,543–24,565, 1998.

Wald, D. J., and T. H. Heaton, Spatial and temporal distribution of slip for the 1992 Landers, California, earthquake, *Bull. Seism. Soc. Am.*, *84*, 668–691, 1994.

———————

J. McCloskey, S. S. Nalbant, and S. Steacy, Geophysics Research Group, School of Biological & Environmental Sciences, University of Ulster, Coleraine, Co.Derry BT52 1SA Northern Ireland. (J.McCloskey@ulster. ac.uk; S.Steacy@ulster.ac.uk; SS.nalbant@ulster.ac.uk)

C. Nostro, Istituo Nazionale di Geofisica et Volcanologia, Via di Vigna Murata 605 I-00143 Roma, Italy.

O. Scotti and D. Baumont, Institut de Protection et Surete Nuclaire (IPSN) -DPRE BP 6 F-92265 Fontenay-Aux-Roses, France.